ELSEVIER

Computational Materials Science 22 (2001) 240–260

COMPUTATIONAL MATERIALS SCIENCE

www.elsevier.com/locate/commatsci

Thermodynamic–kinetic simulation of solidification in binary fcc copper alloys with calculation of thermophysical properties

J. Miettinen *

Laboratory of Metallurgy, Helsinki University of Technology, P.O. Box 6200, FIN-02015 Hut, Finland

Accepted 1 June 2001

Abstract

A thermodynamic–kinetic model is presented for the simulation of phase change and solute redistribution during solidification of binary, one-solid-phase (fcc) copper alloys containing Ag, Al, Ni, P, Sn or Zn. Depending on the alloy composition, the cooling rate and the dendrite arm spacing, the model determines the phase fractions and compositions during solidification. In addition, it calculates important thermophysical material properties (enthalpy, specific heat, thermal conductivity, density and viscosity) from the liquid state down to room temperature. These data are important input data for other models, such as heat transfer and thermal stress models, whose reliability has become more and more dependent on the input data itself. The model is validated comparing calculated results with experimental data of literature.

Keywords: Copper alloys; Kinetics; Material properties; Solidification; Thermodynamics

1. Introduction

Since the 1960s, several models have been developed to simulate solidification and the related solute redistribution in metallic alloys, as reviewed by Rappaz [1] and Flemings [2]. Most of these models assume that the dendritic structure is columnar having some simplified form and that there is no macroscopic solute transport and no local solute gradients in the liquid phase. With these simplifications, the mathematical treatments can be made in one-volume-element located at the side of a dendrite arm. During the last decade, a thermodynamic–kinetic model of interdendritic solidification (IDS) [3–5] was developed for steels. In that model, the main instruments of the conventional solute redistribution models, i.e., the material balance equations and Fick's laws of solute diffusion, were incorporated into a proper set of thermodynamic chemical-potential-equality equations, which relate the phase interface compositions to both the temperature and the phase stabilities. Due to the thermodynamic approach of the model, important enthalpy-related data can be produced for other models simulating the heat transfer in steel castings. The model also calculates other thermophysical properties, such as thermal conductivity, density and viscosity.

This paper shows an IDS-type model for binary copper alloys containing Ag, Al, Ni, P, Sn or Zn. The new model, copper alloy solidification for binary one-solid-phase alloys (CASBOA), determines the fractions and compositions of the liquid and solid (fcc) phase at any temperature during solidification. In addition, the model calculates

* Tel.: +358-9-773-5148; fax: +358-9-773-5148.

0927-0256/01/$ - see front matter
PII: S0927-0256(01)00239-7

thermophysical material properties, i.e., enthalpy, specific heat, thermal conductivity, density and viscosity, from the liquid state down to room temperature. These data can be used as input data for other models simulating the heat transfer in copper alloy castings.

In the following, the principles of the calculation strategy are presented (Section 2) and algorithms and data are shown and validated for the calculation of thermophysical material properties (Section 3). Next, sample calculations are presented for pure copper and some binary copper alloys (Section 4) and the results of model are compared with some experimental data of solidification (Section 5). Finally, a thermodynamic model and data applied in the CASBOA model are presented (Appendix A) and earlier optimised data of solute diffusion and dendrite arm spacing [6] are shown and validated with experimental data (Appendices B and C).

2. Simulation of solidification

The CASBOA model simulates the fcc solidification of binary copper alloys containing Ag, Al, Ni, P, Sn or Zn. All calculations are made stepwise in one volume element set on the side of a dendrite arm (Fig. 1). This one-volume-element method is typical for most solute redistribution models and is based on the following assumptions [3]:

- The dendritic structure is regular and has a hexagonal arm arrangement.
- There is no solute change between the volume element and its surroundings.
- There is complete solute mixing (no local solute gradients) in the liquid phase.

The simulations in the volume element are also based on certain assumptions. The most important of them greatly simplifying the mathematical treatment are:

- Thermodynamic equilibrium is reached at the fcc/liquid phase interface.
- The difference in the molar volumes of the liquid and fcc phases is negligible.
- No undercooling is required before the formation of fcc phase from the liquid phase.

The equations of the simulation are divided into equations dealing with the thermodynamic equilibrium at the phase interface (Section 2.1) and those dealing with the solute diffusion in the solid phase (Section 2.2). The calculations are made

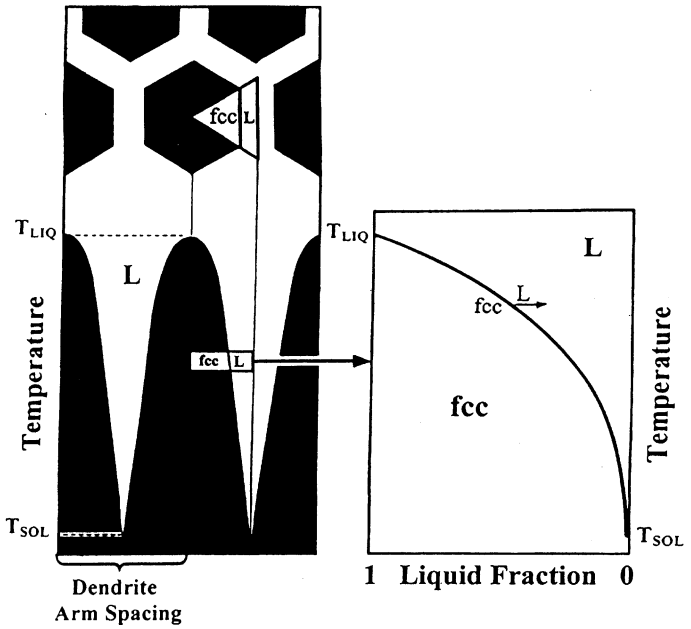

Fig. 1. Volume element on the side of a dendrite arm during the fcc solidification.

stepwise [3] in three phase regions, L (liquid state), L + fcc (mushy zone) and fcc (solid state) (Section 2.3). In regions L and fcc, the temperature is decreased with steps ΔT whereas in region L + fcc, the liquid fraction is decreased with steps Δf_j. In the latter case, a step division of $\Delta f_j = 0.0208$ for $1 \leqslant j \leqslant 5, \Delta f_j = (90 - j) \cdot 0.00025$ for $6 \leqslant j < 87$ and $\Delta f_j = 0.005$ for $j = 87$ was chosen, to get an accurate description of the fcc/L interface movement in the liquid end of the volume element.

2.1. Equations of thermodynamic equilibrium

The thermodynamic equilibrium at the fcc/L interface is determined with the chemical-potential-equality equations as:

$$\mu_{\mathrm{Cu}}^{\mathrm{L}}(T, x_{\mathrm{B}}^{\mathrm{L}}) = \mu_{\mathrm{Cu}}^{\mathrm{fcc}}(T, x_{\mathrm{B}}^{\mathrm{fcc}}), \tag{1}$$

$$\mu_{\mathrm{B}}^{\mathrm{L}}(T, x_{\mathrm{B}}^{\mathrm{L}}) = \mu_{\mathrm{B}}^{\mathrm{fcc}}(T, x_{\mathrm{B}}^{\mathrm{fcc}}), \tag{2}$$

where μ_i^{ϕ} is the chemical potential of component i in phase ϕ, T is the temperature, and $x_{\mathrm{B}}^{\mathrm{L}}$ and $x_{\mathrm{B}}^{\mathrm{fcc}}$ are the compositions (in mole fraction) of solute B at the phase interface (Fig. 1). Terms μ_i^{ϕ} based on the substitutional solution model [7] are defined in Appendix A. Appendix A also shows the proper thermodynamic data for their calculation, based on recent thermodynamic assessments of binary Cu–B systems (B = Ag, Al, Ni, P, Sn, Zn).

2.2. Equations of solute diffusion

For the simulation of interdendritic solidification, one also needs a material balance equation for the determination of compositional changes in the volume element, resulting from the phase interface movement. Assuming a hexagonal arrangement for the dendrite arms (Fig. 1), the following material balance equation was derived for the fcc/L interface:

$$\Delta f^{\mathrm{L}}(x_{\mathrm{B}}^{\mathrm{L0}} - x_{\mathrm{B}}^{\mathrm{fcc}}) = f^{\mathrm{L}}(x_{\mathrm{B}}^{\mathrm{L}} - x_{\mathrm{B}}^{\mathrm{L0}}) - S_{\mathrm{B}}^{\mathrm{fcc/L}}(T,\ x_{\mathrm{B}}^{\mathrm{fcc}},\ D_{\mathrm{B}}^{\mathrm{fcc}}). \tag{3}$$

Here, f^{L} is the liquid fraction, Δf^{L} is the fractional movement of the fcc/L interface, $x_{\mathrm{B}}^{\mathrm{fcc}}$ is the fcc interface composition and $x_{\mathrm{B}}^{\mathrm{L0}}$ is the liquid composition before movement Δf^{L} (Fig. 2). Term $S_{\mathrm{B}}^{\mathrm{fcc/L}}$ includes Fick's first law of diffusion and describes the amount of material in the fcc phase leaving the fcc/L interface (Fig. 2). Its general form is $S_{\mathrm{B}}^{\mathrm{fcc/L}} = 4 \cdot D_{\mathrm{B}}^{\mathrm{fcc}} \cdot \Delta t \cdot G_{\mathrm{B}}^{\mathrm{fcc/L}}/d^2$, where $D_{\mathrm{B}}^{\mathrm{fcc}}$ is the diffusion coefficient of solute B in the fcc phase, Δt is the time increment spent during the fractional movement of the fcc/L interface, $G_{\mathrm{B}}^{\mathrm{fcc/L}}$ is the concentration gradient at the fcc/L interface and d is the dendrite arm spacing. Time increment Δt is related to temperature T as $\Delta t = (T^0 - T)/\dot{T}$, where T^0 is the temperature of the previous calculation step and $\dot{T}$ is the cooling rate. Concentration gradient $G_{\mathrm{B}}^{\mathrm{fcc/L}}$ is related to the interface composition $x_{\mathrm{B}}^{\mathrm{fcc}}$ as $G_{\mathrm{B}}^{\mathrm{fcc/L}} = (x_{\mathrm{B}}^{\mathrm{fcc}} - x_{\mathrm{B}}^{\mathrm{fcc'}})/(\sqrt{f^{\mathrm{fcc/L}}} - \sqrt{f^{\mathrm{fcc/L'}}})$, where $x_{\mathrm{B}}^{\mathrm{fcc'}}$ is the composition at distance $\sqrt{f^{\mathrm{fcc/L}}} - \sqrt{f^{\mathrm{fcc/L'}}}$ from the fcc/L interface ($f^{\mathrm{fcc/L}}$ is the fraction from the dendrite axis to the position of the fcc/L interface and $f^{\mathrm{fcc/L'}}$ is the fraction from the dendrite axis to the position where composition equals to $x_{\mathrm{B}}^{\mathrm{fcc'}}$). As $x_{\mathrm{B}}^{\mathrm{fcc'}}$ can be obtained from the concentration profile resulting from the diffusion simulation with Fick's 2nd law (shown later in this section), parameter $S_{\mathrm{B}}^{\mathrm{fcc/L}}$, in fact, becomes a function of temperature T, interface composition $x_{\mathrm{B}}^{\mathrm{fcc}}$ and diffusion coefficient $D_{\mathrm{B}}^{\mathrm{fcc}}$, as shown by Eq. (3). It also becomes a function of cooling rate $\dot{T}$ and dendrite arm spacing d but these are known as input values of the model.

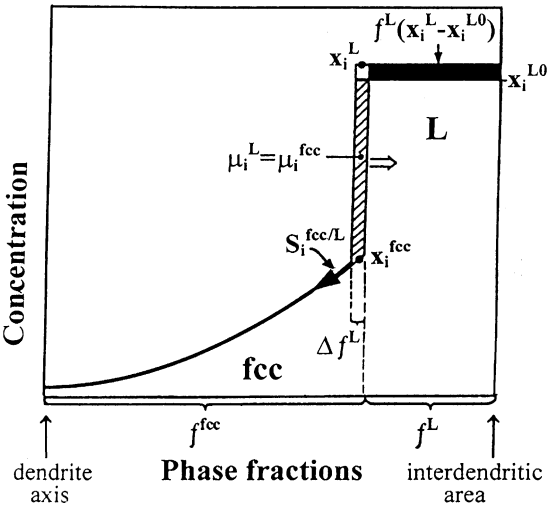

Fig. 2. Change of the solute material balance in the volume element caused by the movement of the fcc/L phase interface.

Finally, one needs so simulate the diffusion of solute B in the fcc phase. This is made applying an implicit finite difference method [3] to the solution of Fick's 2nd law

$$\frac{\partial x_B^{fcc}}{\partial t} = D_B^{fcc} \frac{\partial^2 x_B^{fcc}}{\partial z^2}. \quad (4)$$

As a result, one gets the concentration profile of the solute in the fcc phase.

Proper data for the calculation of diffusion coefficients D_B^{fcc} and dendrite arm spacing d, optimised from the experimental data of literature, are shown in Appendices B and C.

2.3. Strategy of calculation

This section shows how Eqs. (1)–(4) are used in different phase regions, L (liquid state), L + fcc (mushy zone) and fcc (solid state). In addition, in each phase region, the thermophysical material properties are calculated. The proper equations for this are given in Section 3, i.e., only their "call" in different stages of the process is outlined here.

2.3.1. Region L

The solidification of an alloy starts at its liquidus temperature, and in the binary copper alloys of this study, with a formation of the fcc phase. The liquidus temperature ($T = T_{LIQ}$) and the composition of the fcc phase (x_B^{fcc}) are solved from Eqs. (1) and (2) by fixing the liquid composition equal to the nominal composition as $x_B^L = x_B^{nom}$. Then, the temperature is decreased stepwise as $T = T - \Delta T$ from $T_{MAX} = 1300$ °C (maximum temperature of simulation) to the liquidus temperature, and the thermophysical material properties are calculated at each temperature as shown in Section 3. After that, the process is removed to region L + fcc.

2.3.2. Region L + fcc

In region L + fcc, the solidification process is simulated by decreasing the liquid fraction f^L with steps as $f^L = f^L - \Delta f^L$. In every step, parameters T, x_B^{fcc} and x_B^L are solved from Eqs. (1)–(3). After solving these equations, the thermophysical material properties are calculated (Section 3) and the solute diffusion in the fcc phase is simulated with Eq. (4) using time increment $\Delta t = (T^0 - T)/\dot{T}$. The solidification is continued in region L + fcc until, with liquid fraction $f^L \approx 0$, the process is removed to region fcc. When solving Eqs. (1)–(3), note that the value of concentration gradient $G_B^{fcc/L}$ included in function $S_B^{fcc/L}$ must be known in each step. This is estimated from the concentration profile of the solute obtained from the solution of Eq. (4) in the previous step. Exceptionally, if the temperature becomes lower than the temperature of the peritectic or eutectic reaction of the system (taken from the binary phase diagram), the simulation is ended and the solidus temperature is fixed as $T_{SOL} = T_{PHA} - \Delta T'$, where T_{PHA} is the temperature of the formation of a new phase due to the reaction and $\Delta T'$ is a temperature increment determined on the basis of the fcc/L-interface growth history and an estimated increase in the growth during the reaction. In different binary systems, temperature T_{PHA} takes the following values: $T_{PHA} = 777$°C in Cu–Ag (eutectic reaction, Ag-rich fcc phase formed), $T_{PHA} = 1036$ °C in Cu–Al (eutectic reaction, bcc phase formed), $T_{PHA} = 714$°C in Cu–P (eutectic reaction, Cu_3P phase formed), $T_{PHA} = 797$°C in Cu–Sn (peritectic reaction, bcc phase formed) and $T_{PHA} = 902$°C in Cu–Zn (peritectic reaction, bcc phase formed).

2.3.3. Region fcc

In region fcc, temperature is decreased stepwise as $T = T - \Delta T$. At each temperature, the thermophysical material properties are calculated (Section 3) and the solute diffusion in the fcc phase is simulated with Eq. (4) using time increment $\Delta t = \Delta T/\dot{T}$. At room temperature, 25°C, the simulation is ended.

3. Calculation of material properties

If a certain thermophysical material property is known for individual phases, while knowing the fractions and compositions of these phases as a function of temperature (resulting from the CASBOA simulation), one is able to calculate this property for a chosen alloy from the liquid state down to room temperature. Important solidification related thermophysical properties are

enthalpy-related data (enthalpy, specific heat and latent heat of phase change), thermal conductivity, density and viscosity. Algorithms for calculating these properties are described in the following sections.

3.1. Enthalpy-related data

According to the classical thermodynamics, the molar enthalpy (J/mol) and the molar heat capacity (J/K mol) of a system can be expressed as [1]

$$H = G - T\left(\frac{\partial G}{\partial T}\right)_{\mathrm{P}}, \tag{5}$$

$$C_{\mathrm{P}} = -T\left(\frac{\partial^2 G}{\partial T^2}\right)_{\mathrm{P}}, \tag{6}$$

where G is the molar Gibbs energy of the system (J/mol). For a phase mixture containing liquid phase (L) and fcc phase, the molar Gibbs energy can be given as

$$G = f^{\mathrm{L}}G^{\mathrm{L}} + (1 - f^{\mathrm{L}})G^{\mathrm{fcc}}, \tag{7}$$

where f^{L} is the fraction of liquid $(= 1 - f^{\mathrm{fcc}})$ and G^{ϕ} is the molar Gibbs energy of phase ϕ ($\phi = \mathrm{L}, \mathrm{fcc}$), both obtained from CASBOA calculations. For a binary copper alloy, G^{ϕ} is expressed as shown in Appendix A. Finally, knowing H and C_{P} of Eqs. (5) and (6), one can approximate the latent heat of solidification as

$$L = H(T_{\mathrm{LIQ}}) - H(T_{\mathrm{SOL}}) - \int_{T_{\mathrm{SOL}}}^{T_{\mathrm{LIQ}}} C_{\mathrm{P}}\,\mathrm{d}T, \tag{8}$$

where T_{LIQ} and T_{SOL} are the liquidus and solidus temperatures of the alloy. When applying the enthalpy-related data to heat transfer calculations, one may use either the enthalpy function of Eq. (5) directly or the heat capacity function of Eq. (6) with the latent heat value calculated from Eq. (8). Assessed thermodynamic data for the calculation of G^{ϕ}, and finally, H, C_{P} and L via Eqs. (5)–(8), are shown in Appendix A.

3.1.1. Validation of enthalpy-related data derived from thermodynamic data

As stated above, the enthalpy-related data can be derived from the assessed thermodynamic data shown in Appendix A. As the assessed data are always validated with experimental measurements, such as those of phase equilibrium, component activity and mixing enthalpy, they should represent the best possible description of the overall thermodynamic properties of the system. However, as the common (and reasonable) trend is to apply a minimum amount of calculation parameters in the assessments, it is sometimes impossible to get good agreement with all the available experimental data. It is quite common that the assessor has to favour some experimental measurements in regard to some other measurements. Hence, if no emphasis or only little emphasis was given on the enthalpy measurement of the system, there is a risk that the thermodynamic data does not give a reliable estimation of enthalpy in that system. In the earlier study [8], it was checked whether this is true for certain binary Cu–B alloys (B = Ag, Al, Fe, Mn, Ni, Si, Sn and Zn) for which experimental enthalpy-related data are available. In the following, the same procedure is repeated for pure copper and those Ag, Al, Ni, Sn and Zn containing copper alloys solidifying in the fcc mode only.

First, enthalpy-temperature functions $H(T)$ were calculated for pure copper and binary copper alloys containing 5%Al, 10%Ni, 20%Ni, 30%Ni, 40%Ni, 5%Sn, 10%Sn, 4.5%Zn, 10.9%Zn, 18.7%Zn, 23.2%Zn and 29.7%Zn (all compositions in wt% except for Zn in at.%). The experimental enthalpy data are from [9] for pure copper, from [10] for Cu–Zn alloys and from [11] for the other alloys. The calculations were carried out as follows. In one-phase region ϕ (L and fcc), $f^{\phi} = 1$ and Eq. (A.1) of Appendix A was directly inserted into Eq. (5) to calculate H. In the case of pure copper, $x_{\mathrm{B}}^{\phi} = 0$ (i.e., $x_{\mathrm{Cu}}^{\phi} = 1$), and in the case of alloys, $x_{\mathrm{B}}^{\phi} = x_{\mathrm{B}}^{\mathrm{NOM}}$ (nominal composition of the alloy). In

[1] For heat transfer models, H and C_{P} are usually given in units J/g and J/g K, respectively. In the latter case, C_{P} is called as specific heat. The proper unit conversion is made dividing the original H value (J/mol) and C_P value (J/K mol) with the molar weight of the alloy, M (g/mol). This is defined as $M = (1 - x_{\mathrm{B}}^{\mathrm{NOM}}) \cdot M_{\mathrm{Cu}} + x_{\mathrm{B}}^{\mathrm{NOM}} \cdot M_{\mathrm{B}}$, where M_{Cu} and M_{B} are the molar weights of pure copper and component B, respectively, and $x_{\mathrm{B}}^{\mathrm{NOM}}$ is the nominal composition (mole fraction) of component B in the alloy.

two-phase region L + fcc (alloys only), compositions x_B^L and x_B^{fcc} were solved with Eqs. (1) and (2), liquid fraction f^L was calculated as $f^L = (x_B^{NOM} - x_B^{fcc})/(x_B^L - x_B^{fcc})$ (equilibrium solidification), G^L and G^{fcc} were calculated by Eq. (A.1) of Appendix A, G was calculated by Eq. (7), and H was calculated by Eq. (5). By making these one-phase and two-phase calculations as a function of temperature, enthalpy functions $H(T)$ were obtained for pure copper and the binary alloys (in each case, enthalpy was expressed relative to the enthalpy of first experimental data point in the liquid phase). Table 1 shows the average error between the experimental and calculated enthalpy data. The average error term in the last column is defined as $100 \cdot \Sigma(|H^{exp} - H^{cal}|)/n/H^{exp,MAX}$, where the summation covers the n experimental data points of the alloy and $H^{exp,MAX}$ is the maximum experimental enthalpy value of the data (note that $H^{exp,MAX}$ was applied as a divisor since H^{exp} may equal to zero). As can be seen, the agreement is reasonable for any alloy.

Table 1
Average error between the experimental and calculated enthalpy data for pure copper and binary copper alloys (shown also are the number of the experimental data points and the temperature ranges of the data)

Alloy	Data points	T (°C)	Average error (pct)
Cu	17	25–1427	0.4
Cu + 5wt%Al	33	122–1203	2.0
Cu + 5wt%Sn	30	122–1203	0.9
Cu + 10wt%Sn	26	122–1203	0.9
Cu + 10wt%Ni	25	367–1217	0.4
Cu + 20wt%Ni	26	367–1253	1.3
Cu + 30wt%Ni	28	367–1296	2.2
Cu + 40wt%Ni	28	367–1323	2.4
Cu + 4.5at.%Zn	12	127–1112	1.4
Cu + 10.9at.%Zn	12	127–1112	2.4
Cu + 18.7at.%Zn	10	127–1032	4.1
Cu + 23.2at.%Zn	12	127–1067	0.7
Cu + 29.7at.%Zn	12	127–1097	1.3

Next, mixing enthalpies, H_{MIX}^{ϕ}, were calculated for binary liquid copper systems containing Ag, Al, Ni, Sn and Zn, and binary fcc copper systems containing Ni and Zn. The experimental enthalpy data of these systems are from [10,12–27] for the liquid phase, and from [10,28–34] for the fcc phase. The calculations were carried out with Eq. (5), by inserting Eq. (A.2) of Appendix A with $\phi = L$ and $\phi = fcc$ into it. Table 2 shows the average error between the experimental and calculated mixing enthalpy data for each system. The average error term in the last column is defined as $100 \cdot \Sigma(|H_{MIX}^{exp} - H_{MIX}^{cal}|)/n/H_{MIX}^{exp,MAX}$, where the summation covers the n experimental data points of the system and $H_{MIX}^{exp,MAX}$ is the maximal experimental mixing enthalpy value of the data (note that $H_{MIX}^{exp,MAX}$ was applied as a divisor since since H_{MIX}^{exp} may equal to zero). As can be seen, the agreement is reasonable for most systems. For the liquid Cu–Al system and the fcc Cu–Ni system, the agreement was quite moderate but this is only due to the scatter in the experimental data. In fact, even in these systems, the calculated data well represented the average (though scattered) behaviour of the experimental data.

A test was also made for heat capacity, by calculating heat capacity functions $C_P(T)$ for binary Cu–B alloys containing 3%Al, 30%Ni, 40%Ni, 10%Zn and 30%Zn (all compositions in wt%). The experimental heat capacity data of these alloys are from [35–37]. The calculations were

Table 2
Average error between the experimental and calculated mixing enthalpy data for the liquid and fcc phases of binary copper systems (shown also are the number of the experimental data points, and the composition and the temperature ranges of the data)

System Cu–B	Phase	Data points	x_B	T (°C)	Average error (pct)
Cu–Ag	L	34	0.01–0.4	1100–1102	2.4
Cu–Al	L	20	0.08–0.5	1100–1427	15.2
Cu–Ni	L	20	0.025–0.515	1200–1480	7.7
Cu–Sn	L	33	0.025–0.5	724–1167	9.1
Cu–Zn	L	12	0.045–0.5	1000–1127	6.7
Cu–Ni	fcc	14	0.025–0.42	500–1000	12.1
Cu–Zn	fcc	36	0.015–0.365	25–327	4.8

carried out as for the enthalpy functions $H(T)$ described above. In each alloy, good agreement was obtained between the calculated and experimental heat capacity data.

Finally, calculated latent heat of pure copper was compared with the experimental data of literature [9–11,17,38–40]. The calculated value, $L = 13\,263$ J/mol, exactly equals to the average experimental value of these seven studies.

3.2. Thermal conductivity

Knowing the liquid fraction f^L from the CASBOA simulation, the thermal conductivity of an alloy is calculated as

$$k = (1 - f^L)k^{fcc} + A \cdot f^L k^L, \quad (9)$$

where k^L and k^{fcc} are the thermal conductivities of the liquid and fcc phases, and A is a constant-value parameter describing the effect of convection upon the thermal conductivity of liquid (e.g., with $A = 1$, there is no effect due to convection). In the following sections, specific functions are optimised for k^L and k^{fcc}, using experimental data of literature.

3.2.1. Liquid phase

There is little information of the thermal conductivity in liquid copper alloys [41]. In the present study, these data were fitted to the form of the following function:

$$k^L = a_{Cu} + b_{Cu}T + c_{Cu}T^2 + (a_B + b_B T + c_B T^2)C_B^L + d_B C_B^L \cdot 10^{-n_B C_B^L}, \quad (10)$$

where k^L is in W/K m, temperature T is in °C and composition C_B^L is in wt%. The form of Eq. (10) was chosen due to the observed tendency of solutes to decrease thermal conductivity drastically at low solute contents but less drastically with increasing solute contents. In the CASBOA simulation, C_B^L represents the nominal liquid composition before the solidification and the interdendritic liquid composition during the solidification. Parameters a, b, c, d and n for copper and different solutes were solved with the regression analysis and their values are shown in Table 3. In the case of Ag, the parameters were exceptionally derived from the tabulated thermal conductivity data of pure Cu [41] and pure Ag [42]. In the case of phosphorus, one should notice that Eq. (10) yields reasonable results up to the content of 1 wt% P only.

Table 3
Parameters a, b, c, d and n of Eq. (10) for the calculation thermal conductivity (W/K m) in pure liquid copper and binary liquid copper alloys

	a	b	c	d	n
Cu	134.407	0.026743	0		
Ag	−0.005	0.000159	0	0	0
Al	−2.654	0	0	−16.162	0.04
Ni	−2.654	0	0	−12.122	0.04
P	0	0	0	−486.360	0.50
Sn	−2.474	0	0	−14.779	0.04
Zn	−2.118	0	0	−14.942	0.04

3.2.2. Fcc phase

Also in fcc copper alloys, increasing solute contents decrease the value of thermal conductivity drastically, but no longer at high solute contents. Using the experimental data of pure fcc copper [43] and fcc copper alloys [42,44–46], the following function was optimised for the calculation of thermal conductivity in the fcc phase:

$$k^{fcc} = a_{Cu} + b_{Cu}T + c_{Cu}T^2 + (a_B + b_B T + c_B T^2)C_B^{fcc} + (d_B + e_B T)C_B^{fcc} \cdot 10^{-n_B C_B^{fcc}}. \quad (11)$$

In the equation, k^{fcc} is in W/K m, temperature T is in °C and composition C_B^{fcc} is in wt%. In the CASBOA simulation, C_B^{fcc} represents the average fcc composition obtained from the concentration profile. Parameters a, b, c, d, e and n for copper and different solutes were solved with the regression analysis and their values are shown in Table 4. It is worth noticing that for Cu–Ag, Cu–P and Cu–Sn alloys, an artificial temperature dependency, comparable to that of other alloys, was estimated. This is just due to the lack of high temperature for these alloys. In the case of phosphorus, one should notice that Eq. (11) yields reasonable results up to the content of 0.2 wt% P only.

Table 4
Parameters a, b, c, d, e and n of Eq. (11) for the calculation thermal conductivity (W/K m) in pure fcc copper and binary fcc copper alloys

	a	b	c	d	e	n
Cu	398.61	−0.042062	−0.0000205			
Ag	−11.60	0	0	−80.227	0.034394	0.20
Al	−20.19	0.005341	0	−163.419	0.092412	0.11
Ni	−7.80	0.001537	0	−63.9730	0.027815	0.039
P	−274.385	0	0	−2284.447	1.856380	2.00
Sn	−15.61	0	0	−126.177	0.125745	0.08
Zn	−5.11	0.001901	0	−32.046	0.030979	0.03

Table 5
Average error between the experimental and calculated thermal conductivity data for liquid and fcc phases of pure copper and copper alloys (shown also are the number of the experimental data points and the composition and temperature ranges of the alloys)

Cu–B	Phase	Data points	wt% B	T (°C)	Error (%)
Cu	L	6		1100–1350	0
Cu–Ag	L	2	100	1100–1250	0
Cu–Al	L	2	6.5	1100–1250	4.8
Cu–Ni	L	2	10	1100–1250	2.6
Cu–P	L	2	0.05	1100–1250	1.4
Cu–Sn	L	2	10	1100–1250	0.9
Cu–Zn	L	4	5–30	1100–1250	0.4
Cu	fcc	10		27–927	0.1
Cu–Ag	fcc	1	0.1	20	0
Cu–Al	fcc	14	3–15	27–927	5.7
Cu–Ni	fcc	23	5–40	27–927	11.8
Cu–P	fcc	5	0–0.05	20	3.7
Cu–Sn	fcc	14	1.3–14	20	17.0
Cu–Zn	fcc	20	1–40	20–427	3.4

3.2.3. Validation of optimised thermal conductivity data

Table 5 shows the average error between the experimental and calculated thermal conductivity data. The error term in the last column is defined as $100 \cdot \Sigma(|k^{\exp} - k^{\mathrm{cal}}|/k^{\exp})/n$, where the summation covers the n experimental data points of the system. The agreement is relatively good, when taking into account the scatter in the original experimental data.

3.3. Density

Knowing the liquid fraction f^{L} from the CASBOA simulation, the density of an alloy is calculated as

$$\rho = 1 \Big/ \left(\frac{f^{\mathrm{L}}}{\rho^{\mathrm{L}}} + \frac{1 - f^{\mathrm{L}}}{\rho^{\mathrm{fcc}}} \right), \tag{12}$$

where ρ^{L} and ρ^{fcc} are the densities of the liquid and fcc phases. Further, Eq. (12) can be used to calculate the contraction between temperatures T_1 and T_2 as $\beta(\%) = 100[1 - \rho_{T1}/\rho_{T2}]$. For example, by setting $T_1 = T_{\mathrm{LIQ}}$ and $T_2 = T_{\mathrm{SOL}}$, one gets the contraction in the whole mushy zone (mostly compensated by the liquid feeding) and by setting $T_1 = T_{\mathrm{ZST}}$ and $T_2 = T_{\mathrm{SOL}}$, one gets the contraction in the non-liquid-feeding region of the mushy zone. In the following sections, specific functions are optimised for ρ^{L} and ρ^{fcc}, by using the experimental data of literature.

3.3.1. Liquid phase

The experimental density data of pure liquid copper [39,47–51] and binary liquid copper alloys containing Ag, Al, Ni, P, Sn and Zn [51–54] were fitted to the form of the following function:

$$\rho^{L} = a_{Cu} + b_{Cu}T + c_{Cu}T^2 + (a_B + b_BT + c_BT^2 + d_BC_B^L + e_BC_B^{L2})C_B^L, \quad (13)$$

where ρ^L is in kg/m^3, temperature T is in °C and composition C_B^L is in wt%. In the CASBOA simulation, C_B^L represents the nominal liquid composition before the solidification and the interdendritic liquid composition during the solidification. Parameters a, b, c, d and e for copper and different solutes were solved with the regression analysis and their values are shown in Table 6.

As can be seen, the binary data of liquid copper alloys were taken from one researcher only [51–54]. Data are available also from other studies [47,50,55] but as these data are only partly consistent with Freeman's data and their amount is small, all data were decided to take from Freeman.

3.3.2. Fcc phase

Knowing the lattice spacing of the solid structure of a pure component or alloy, its density can be calculated as $\rho^S = 10^{-3}$ (nM)/(N_0V_T) where density ρ^S is in kg/m^3, n is the number of atoms in the unit cell ($n = 4$ for the fcc structure and $n = 2$ for the bcc structure), M is the molar weight of a pure component or alloy in g/mol and N_0 is the Avogadro's number. Parameter V_T is the volume of the unit cell in m^3 given in lattice spacing terms kX as $V_T = kX^3 \cdot 10^{-30}$ (old method with $N_0 = 6.060 \times 10^{23}$) or in lattice spacing terms$a$ as $V_T = a^3$ (new method with $N_0 = 6.023 \times 10^{23}$ and a in m). The reader is guided to [56] to get more detailed information of these alternative methods.

In the present study, equation $\rho^S = 10^{-3}$ (nM)/(N_0V_T) was used to calculate fcc density data from the experimental lattice spacing data of pure fcc copper and binary fcc copper alloys [57–80]. Fcc density data were also calculated from the experimental linear thermal expansion data of binary fcc copper alloys [42,44,46], by using relation $\alpha = [(\rho_{T0}/\rho_{T1})^{1/3} - 1]/(T_1 - T_0)$, where α is the linear thermal expansion coefficient (1/K) between temperatures $T_1 = 300$°C and $T_0 = 20$°C, and ρ_{T1} and ρ_{T0} are the densities at these temperatures. Using all these density data, the following function was optimised for the calculation of the density in fcc phase:

$$\rho^{fcc} = a_{Cu} + b_{Cu}T + c_{Cu}T^2 + (a_B + b_BT + c_BT^2 + d_BC_B^{fcc})C_B^{fcc}. \quad (14)$$

In the equation, ρ^{fcc} is in kg/m^3, temperature T is in °C and composition C_B^{fcc} is in wt%. In the CASBOA simulation, C_B^{fcc} represents the average fcc composition obtained from the concentration profile. Parameters a, b, c and d for copper and different solutes were solved with the regression analysis and their values are shown in Table 7.

3.3.3. Validation of optimised density data

Table 8 shows the average error between the experimental and calculated density data. The average error term in the last column is defined as $100 \cdot \Sigma(|\rho^{exp} - \rho^{cal}|/\rho^{exp})/n$, where the summation covers the n experimental data points of the system. The agreement is relatively good, when taking into account the scatter in the original experimental data.

3.4. Liquid viscosity

For the calculation of liquid viscosity, in metallic melts, Sichen et al. [81] proposed equation

Table 6
Parameters a, b, c, d and e of Eq. (13) for the calculation density (kg/m^3) in pure liquid copper and binary liquid copper alloys

	a	b	c	d	e
Cu	7552.21	1.061386	−0.000668		
Ag	36.96	−0.010704	0	−2.234942	0.095992
Al	−3.91	−0.028121	0	−11.781294	0.437851
Ni	46.86	−0.015849	0	−0.818378	0.009665
P	−3.00	−0.083823	0	−5.037389	0.833574
Sn	2.73	0.006429	0	−1.307482	0.023920
Zn	0.40	−0.010386	0	−0.420671	0.005943

Table 7
Parameters a, b, c and d of Eq. (14) for the calculation density (kg/m^3) in pure fcc copper and binary fcc copper alloys

	a	b	c	d
Cu	8945.62	−0.460976	−0.0000614	
Ag	4.93	0	0	1.152192
Al	−165.27	0.010000	0	2.523673
Ni	1.48	0.000864	0.000002	−0.025464
P	−119.48	0	0	4.743825
Sn	−1.46	−0.005569	0.000010	0.121010
Zn	−12.45	−0.000804	0	−0.035801

Table 8
Average error between the experimental and calculated density data for the liquid and fcc phases of pure copper and binary copper alloys (shown also are the number of the experimental data points, and the composition and temperature ranges of the data)

Cu–B	Phase	Data points	wt% B	T (°C)	Error (%)
Cu	L	15		1100–1600	0.5
Cu–Ag	L	23	3.6–17.5	1020–1341	0.2
Cu–Al	L	30	1.8–15.1	1080–1360	0.8
Cu–Ni	L	16	8.9–40.7	1168–1466	0.3
Cu–P	L	32	0.03–4.9	1000–1312	0.3
Cu–Sn	L	17	3.7–38.4	802–1392	0.2
Cu–Zn	L	21	4.2–44.3	906–1123	0.2
Cu	fcc	15		18–871	0
Cu–Ag	fcc	16	1.3–9.5	20	0
Cu–Al	fcc	14	0.6–11.8	20	0.1
Cu–Ni	fcc	19	7.1–44.8	20–400	0.1
Cu–P	fcc	4	0.6–1.6	20	0
Cu–Sn	fcc	31	0.9–15.5	20–672	0.1
Cu–Zn	fcc	27	0.5–39.0	20–871	0.1

$$\eta = 1000 \cdot \frac{hN\rho^{\mathrm{L}}}{M} \exp(\Delta G^*/RT), \tag{15}$$

where viscosity η is in Pa s, h is Planck's constant (6.626×10^{-34} J s), N is Avogadro's number (6.023×10^{23} mol^{-1}), ρ^{L} is the liquid density in kg/m^3, M is the molar weight in g/mol, ΔG^* is the Gibbs energy of activation in J/mol, R is the gas constant (8.3145 J/mol K) and T is temperature in K. Eq. (15) can be applied to binary copper melts by calculating ρ^{L} from Eq. (13), M as $M = (1 - x_{\mathrm{B}}^{\mathrm{L}})M_{\mathrm{Cu}} + x_{\mathrm{B}}^{\mathrm{L}}M_{\mathrm{B}}$ ($x_{\mathrm{B}}^{\mathrm{L}}$ is the mole fraction of component B in the liquid phase and M_i is the molar weight of pure component i) and ΔG^* from equation [81]

$$\Delta G^* = (1 - x_{\mathrm{B}}^{\mathrm{L}})\Delta G_{\mathrm{Cu}}^* + x_{\mathrm{B}}^{\mathrm{L}}\Delta G_{\mathrm{B}}^* + c \cdot \left[(1 - x_{\mathrm{B}}^{\mathrm{L}})RT\ln(1 - x_{\mathrm{B}}^{\mathrm{L}}) + x_{\mathrm{B}}^{\mathrm{L}}RT\ln x_{\mathrm{B}}^{\mathrm{L}} + {}^{\mathrm{E}}G^{\mathrm{L}}\right]. \tag{16}$$

In Eq. (16), ΔG_i^* is the Gibbs energy of activation for a pure liquid component, c is a correction coefficient for the mixing effect on ΔG^* (fixed in the present study as $c = 0.5$ to improve the correlation between the calculated and experimental results) and ${}^{\mathrm{E}}G^{\mathrm{L}}$ is the Gibbs excess energy of the liquid phase calculated with Eq. (A.2) of Appendix A. Finally, one has to know the values of parameters ΔG_i^* (i = Cu, Ag, Al, Ni, P, Sn, Zn). Following the treatment of Sichen et al., these were determined as

$$\Delta G_i^* = a + bT, \tag{17}$$

where temperature T is in K, by setting $\Delta G^* = \Delta G_i^*$ and $M = M_i$ in Eq. (15), and by applying the experimental η and ρ^{L} functions of pure liquid components [42,82–86] in that equation. The values of parameters a and b obtained for different components are shown in Table 9. In the CASBOA simulation, composition $x_{\mathrm{B}}^{\mathrm{L}}$ of Eq. (16) and

Table 9
Parameters a and b of Eq. (17) for the calculation of the Gibbs energy of activation of pure liquid components (J/mol)

	a	b
Cu	22 153	20.878
Ag	18 647	24.951
Al	11 831	17.811
Ni	35 184	17.608
Sn	5516	25.437
Zn	10 021	22.660
P	12 884	0

C_B^L of Eq. (13) equal to the nominal liquid composition before the solidification and the interdendritic liquid composition during the solidification.

3.4.1. Validation of optimised liquid viscosity data

Table 10 shows the average error between the experimental [84,87–89] and calculated liquid viscosity data. The error term in the last column is defined as $100 \cdot \Sigma(|\eta^{exp} - \eta^{cal}|/\eta^{exp})/n$, where the summation covers the n experimental data points of the system. The agreement is reasonable except for system Cu–Ni. On the other hand, due to the big uncertainty in the viscosity measurements, it is difficult to draw unambiguous conclusions from the reliability of the calculated results. Besides, the method itself is not yet so well validated, i.e., with a sufficiently large amount of experimental data. As an example, Sichen et al. [81] obtained good results for binary Ag–Sn and Fe–Co systems by using $c = 1$ in Eq. (16) whereas, in the present study, reasonable results were obtained by fixing $c = 0.5$. On this basis, the calculated viscosity data should be regarded as rough approximations only.

Table 10
Average error between the experimental and calculated liquid viscosity data for binary copper alloys (shown also are the number of the experimental data points, and the composition and the temperature ranges of the data)

Cu–B	Data points	wt% B	T (K)	Error (%)
Cu	9		1358–1758	0
Cu–Ag	1	8.26	1358	9.6
Cu–Ni	2	20–40	1673	17.7
Cu–P	1	1.5	1473	4.2
Cu–Sn	3	2.92–19.22	1273–1358	5.8

4. Results of calculations

Figs. 3–8 show calculated results of enthalpy (Fig. 3), specific heat (Fig. 4), thermal conductivity (Fig. 5), density (Fig. 6), liquid viscosity (Fig. 7) and interdendritic composition (Fig. 8) for pure copper and three commercial copper alloys containing 5%Al (aluminium bronze, C60800), 5%Ni (cupronickel, C70400) and 5%Zn (gilding metal, C21000). For each alloy, the applied cooling rate

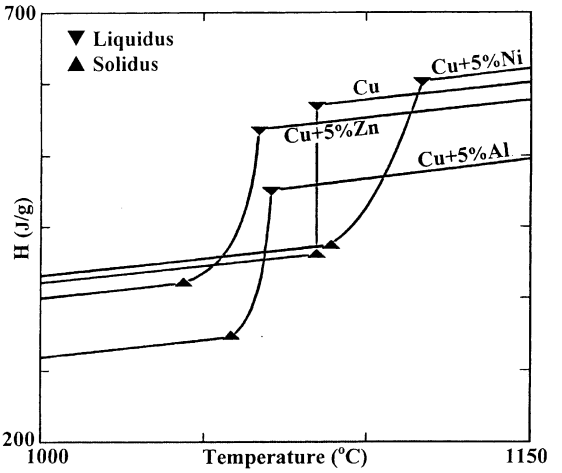

Fig. 3. Calculated enthalpy functions $H(T)$ for pure copper and copper alloys containing 5 wt% Al, Ni and Zn (alloys cooled with a rate of $\dot{T} = 10$°C/s).

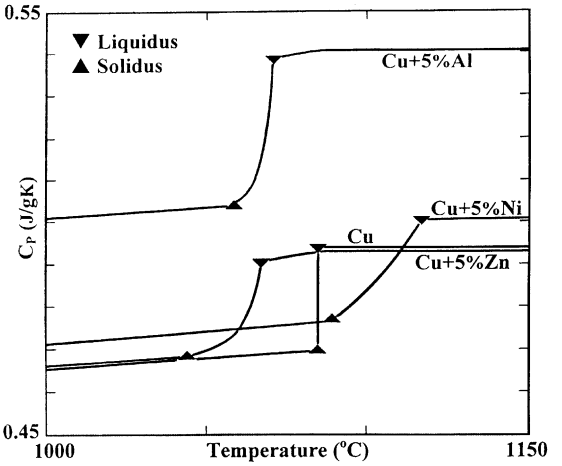

Fig. 4. Calculated specific heat functions $C_P(T)$ for pure copper and copper alloys containing 5 wt% Al, Ni and Zn (alloys cooled with a rate of $\dot{T} = 10$°C/s).

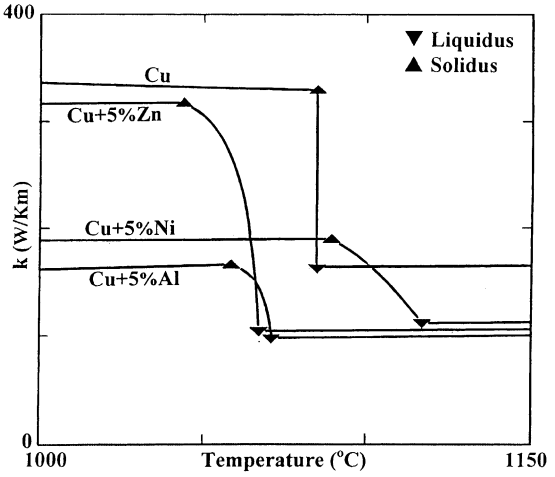

Fig. 5. Calculated thermal conductivity functions $k(T)$ for pure copper and copper alloys containing 5 wt% Al, Ni and Zn (alloys cooled with a rate of $\dot{T} = 10$°C/s).

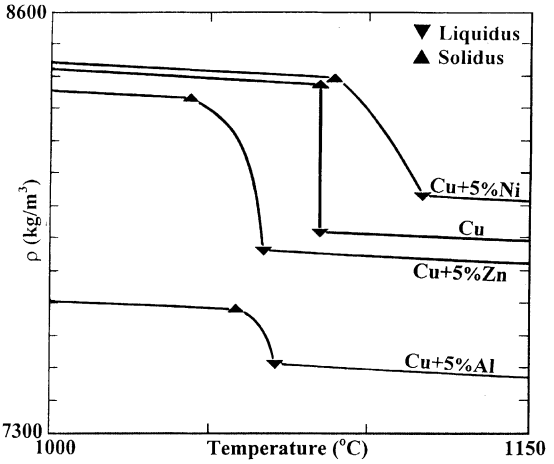

Fig. 6. Calculated density functions $\rho(T)$ for pure copper and copper alloys containing 5 wt% Al, Ni and Zn (alloys cooled with a rate of $\dot{T} = 10$°C/s).

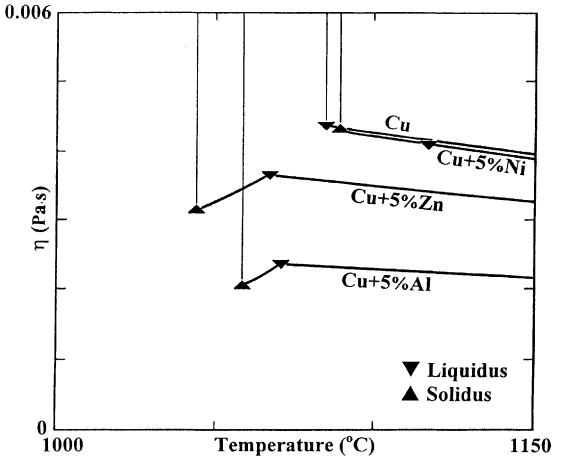

Fig. 7. Calculated liquid viscosity functions $\eta(T)$ for pure copper and copper alloys containing 5 wt% Al, Ni and Zn (alloys cooled with a rate of $\dot{T} = 10$°C/s).

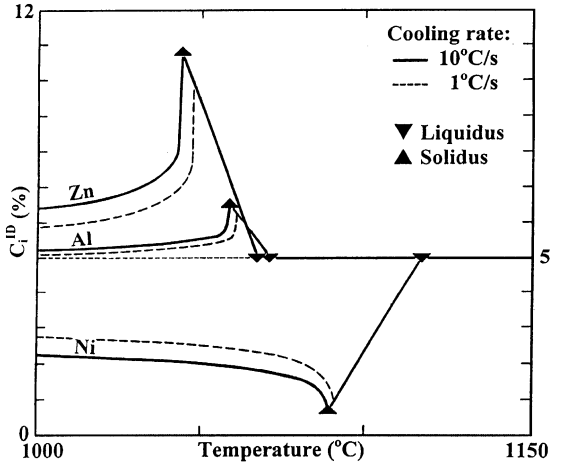

Fig. 8. Calculated interdendritic composition functions $C_i^{\mathrm{ID}}(T)$ for copper alloys containing 5 wt% Al, Ni and Zn (alloys cooled with rates of $\dot{T} = 10$°C/s and $\dot{T} = 1$°C/s).

of simulation was $\dot{T} = 10$°C/s. Via Eq. (C.2) of Appendix C, this resulted in dendrite arm spacings of $d = 59$ μm for Cu + 5%Al, $d = 39$ μm for Cu + 5%Ni and $d = 46$ μm for Cu + 5%Zn, also applied in the simulation. For pure copper, the results represent those of equilibrium solidification, since the present model does not deal with the kinetics in pure substances.

Worth noting in Figs. 3–7 is the different temperature range and location of the mushy zone, causing a different discontinuity in the described material properties in each case. Particularly strong is the effect of 5%Al and 5%Ni alloying on the thermal conductivity of pure copper (Fig. 5): during the solid/liquid phase change, this is increased only slightly, when compared with that of pure copper and the Cu + 5%Zn alloy. Alloying, indeed, has a strong influence on the thermal conductivity in copper. Consequently, results obtained with some commercial heat transfer models are highly dependant on that data, but of course, on the applied enthalpy data also (Fig. 3). In the

case of viscosity (Fig. 7), note the sudden increase in viscosity at the solidus temperature. This is simply due to the disappearance of the liquid phase, i.e., the functions above the solidus describe only the viscosity in the liquid phase, with no effect of solid on that property.

Fig. 8 shows the microsegregation tendency in the studied alloys. In each alloy, the uniform liquid composition before the start of solidification was 5%. During the solidification, the disappearing (interdendritic) liquid phase was enriched by Al and Zn (Zn more strongly than Al) and impoverished by Ni. On the basis of the binary Cu–Zn, Cu–Al and Cu–Ni phase diagrams, this can be explained by the partition coefficient of the solutes, yielding $k_i^{\mathrm{fcc/L}} < 1$ for Al and Zn and $k_i^{\mathrm{fcc/L}} > 1$ for Ni. After the disappearance of the last liquid drop, the interdendritic compositions of Al and Zn "collapsed", i.e., the structure was composition-homogenised quite effectively. This is mainly due to the relatively fast diffusion of Al and Zn in fcc copper. In the case of nickel, the homogenisation remained weaker, just due to the slow diffusion in Ni in fcc copper. The results are shown with two cooling rates, $\dot{T} = 10$°C/s (solid lines) and $\dot{T} = 1$°C/s (broken lines) revealing that the lower the cooling rate (i.e., more time given for the solute diffusion) the more effective the homogenisation. This is partly compensated by the coarser dendrite arms (i.e., longer diffusion distances) obtained with the lower cooling rate, but not much.

Finally, Table 11 shows the important temperatures and properties of pure copper and certain binary copper alloys as a function of the cooling rate. Worth noting in each alloy is the effect of cooling rate on the temperature range of the mushy zone, ΔT. This is increased considerably when increasing the cooling rate. In addition, depending on alloying, different properties vary quite a lot. As an example (in the alloys of Table 11), the mushy zone contraction, β_{MUS}, varies from 2% to 7%, the latent heat of solidification, L, varies from 170 to 240 J/g, the thermal conductivity at the liquidus, k^{L}, varies from 70 to 160 W/K m and the thermal conductivity at the solidus, k^{S}, varies from 90 to 330 W/K m. Again, it is worth emphasizing the role of accurate material data for a reliable a heat transfer simulation.

5. Model validation

Table 12 shows a comparison between calculated and experimental [91] liquidus and solidus temperature data of two binary copper alloys, Cu + 0.022%P and Cu + 29.3%Zn. The agreement is reasonable for both alloys. In addition, calculated microsegregation of Zn of the latter alloy was compared with the experimental measurement [91] (the microsegregation is defined as $I_{\mathrm{Zn}} = C_{\mathrm{Zn}}^{\mathrm{ID}}/C_{\mathrm{Zn}}^{\mathrm{D}}$, where $C_{\mathrm{Zn}}^{\mathrm{ID}}$ is the mean concentration in the interdendritic area and $C_{\mathrm{Zn}}^{\mathrm{D}}$ is the mean concentration in the dendrite centre area). The calculated microsegregation was $I_{\mathrm{ZN}}^{\mathrm{CAL}} = 1.17$ agreeing well with the measured value, $I_{\mathrm{ZN}}^{\mathrm{EXP}} = 1.2$. For other binaries, Cu–Ag, Cu–Al, Cu–Ni and Cu–Sn, no solidus temperature and microsegregation data of non-equilibrium solidification seem to be available. For liquidus temperatures, however, the CASBOA model gives a good estimation in each of the considered binaries, Cu–B (B = Ag, Al, Ni, P, Sn, Zn). This prediction originates in the accurate thermodynamic assessments of these binaries, taken from the literature.

6. Summary

Theory and the aims of a thermodynamic–kinetic solidification model for binary copper alloys containing Ag, Al, Ni, P, Sn and Zn have been presented. The model simulates the fcc/liquid phase change and the related solute redistribution, depending on the alloy composition, cooling rate and dendrite arm spacing. The simulation is based on the use of thermodynamic chemical-potential-equality determining the thermodynamic equilibrium at the phase interface, solute material balance equation related to the movement of the fcc/liquid phase interface and Fick's diffusion laws simulating the solute diffusion in the fcc phase. The calculations are made stepwise in one-volume-element located on the side of a dendrite arm by assuming a hexagonal arrangement for dendrite arms and conditions with negligible convection. As a result, one gets the phase fractions and compositions as a function of temperature.

Table 11
Important temperatures and properties of pure copper and binary copper alloys as a function of cooling rate $\dot{T}$: liquidus temperature (T_{LIQ}), eutectic or peritectic temperature (T_{PHA}), solidus temperature (T_{SOL}), solidification range (ΔT), contraction between liquidus and solidus (β_{MUS}), contraction between zero-strength point and solidus (β_{ZST}), latent heat of solidification (L), thermal conductivity at liquidus (k_{LIQ}) and thermal conductivity at solidus (k_{SOL})[a]

Alloy	$\dot{T}$ (°C/s)	d (μm)	T_{LIQ} (°C)	T_{PHA} (°C)	T_{SOL} (°C)	ΔT (°C)	β_{MUS} (%)	β_{ZST} (%)	L (J/g)	k_{LIQ} (W/K m)	k_{SOL} (W/K m)
Pure Cu	0	–	1085	–	1085	0	5.44	–	209	163	329
Cu + 1%Ag	0	–	1079	–	1059	20	5.36	0.88	206	163	292
1%Ag	1	66	1079	–	1028	51	5.56	1.04	206	163	295
1%Ag	10	31	1079	–	1015	64	5.65	1.13	206	163	296
1%Ag	100	14	1079	–	1000	79	5.75	1.23	206	163	297
Cu + 5%Ag	0	–	1057	–	963	95	5.71	1.19	196	164	258
5%Ag	1	36	1057	–	897	160	6.20	1.57	196	164	262
5%Ag	10	17	1057	–	826	232	6.80	2.12	197	164	268
5%Ag	100	8	1057	777	764	293	7.59	2.88	191	164	262
Cu + 1%Al	0	–	1086	–	1086	0	4.23	0.69	206	146	265
1%Al	1	147	1086	–	1086	0	4.23	0.69	206	146	265
1%Al	10	69	1086	–	1086	0	4.23	0.69	206	146	265
1%Al	100	32	1086	–	1086	0	4.23	0.69	206	146	265
Cu + 5%Al	0	–	1071	–	1067	4	2.09	0.33	198	99	166
5%Al	1	126	1071	–	1060	10	2.13	0.36	198	99	166
5%Al	10	59	1071	–	1059	12	2.14	0.37	198	99	166
5%Al	100	28	1071	–	1057	14	2.16	0.39	198	99	166
Cu + 5%Ni	0	–	1117	–	1106	11	4.19	0.74	216	113	190
5%Ni	1	82	1117	–	1090	27	4.29	0.84	216	113	190
5%Ni	10	39	1117	–	1089	28	4.30	0.85	216	113	190
5%Ni	100	18	1117	–	1088	28	4.30	0.85	216	113	190
Cu + 25%Ni	0	–	1225	–	1182	42	3.01	0.48	242	71	88
25%Ni	1	42	1225	–	1142	82	3.23	0.60	242	71	87
25%Ni	10	20	1225	–	1131	94	3.29	0.65	242	71	87
25%Ni	100	9	1225	–	1122	103	3.33	0.69	242	71	87
Cu + 0.01%P	0	–	1084	–	1082	2	5.43	0.90	209	159	323
0.01%P	1	174	1084	–	1069	15	5.52	0.99	209	159	325
0.01%P	10	82	1084	–	1067	18	5.54	1.01	209	159	325
0.01%P	100	38	1084	–	1064	21	5.55	1.03	209	159	326
Cu + 0.05%P	0	–	1084	–	1072	12	5.49	0.95	208	140	304
0.05%P	1	172	1084	–	1032	52	5.76	1.22	208	140	308
0.05%P	10	81	1084	–	1020	63	5.83	1.30	208	140	309
0.05%P	100	38	1084	–	1007	77	5.92	1.39	208	140	310

Table 11 (Continued)

Alloy	$\dot{T}$ (°C/s)	d (μm)	T_{LIQ} (°C)	T_{PHA} (°C)	T_{SOL} (°C)	ΔT (°C)	β_{MUS} (%)	β_{ZST} (%)	L (J/g)	k_{LIQ} (W/K m)	k_{SOL} (W/K m)
Cu + 1%Sn	0	–	1078	–	1020	58	5.75	1.12	205	147	320
1%Sn	1	158	1078	–	924	155	6.35	1.71	205	147	319
1%Sn	10	74	1078	–	891	188	6.55	1.92	205	147	319
1%Sn	100	35	1078	–	852	227	6.79	2.16	205	147	319
Cu + 5%Sn	0	–	1048	–	910	137	6.30	1.41	193	103	242
5%Sn	1	106	1048	797	790	257	6.96	1.98	193	103	219
5%Sn	10	50	1048	797	784	264	7.00	2.00	193	103	220
5%Sn	100	23	1048	797	779	269	7.02	2.00	193	103	220
Cu + 5%Zn	0	–	1067	–	1061	7	5.49	0.91	203	105	317
5%Zn	1	98	1067	–	1047	20	5.58	0.98	203	105	317
5%Zn	10	46	1067	–	1044	23	5.60	1.00	203	105	317
5%Zn	100	21	1067	–	1041	26	5.62	1.02	203	105	317
Cu + 30%Zn	0	–	949	–	919	31	7.26	1.26	173	68	227
30%Zn	1	53	949	–	905	44	7.36	1.31	173	68	226
30%Zn	10	25	949	902	901	48	7.34	1.26	173	68	225
30%Zn	100	12	949	902	899	50	7.37	1.27	173	68	225

[a] In the table, a zero-value cooling rate denotes equilibrium solidification. The secondary dendrite arm spacing d was calculated by Eq. (C.2) of Appendix C.

Table 12
Experimental [91] and calculated liquidus and solidus temperatures of Cu + 0.022%P and Cu + 29.3%Zn alloys

Alloy	$\dot{T}$ (°C/s)	d_2 (μm)	T_{LIQ} (°C)		T_{SOL} (°C)	
			Exp.	Cal.	Exp.	Cal.
Cu + 0.022%P	0.5	220	1082	1084	1065	1058
	1.2	180	1082	1084	1055	1054
Cu + 29.3%Zn	0.5	160	952	953	885	892
	0.9	150	952	953	880	885

In addition, by using experimental data of literature, specific formulas were optimised to calculate important solidification-related thermophysical material properties for the mentioned copper alloys. The formulas are heavily based on the use of the base model, which solve the phase fractions and compositions needed in these calculations. With these formulas, enthalpy, specific heat, thermal conductivity, density and viscosity can be calculated from the liquid state down to room temperature, taking into account the phase change discontinuity at a specific temperature range influenced by the alloy composition and cooling.

Sample calculations were presented for pure copper and binary copper alloys showing the strong influence of alloying on the thermophysical material data, especially thermal conductivity. No less important is the role of cooling rate determining the solidification range and thus, the discontinuity in the material property in the mushy zone region. On this basis, it is clear that a reliable heat transfer simulation is not possible without accurately determined, temperature dependant thermophysical material data. The calculations were also compared with some experimental data of solidification. The comparison was made for the solidification range and the solute microsegregation in Cu + 0.022%P and Cu + 29.3%Zn alloys showing reasonable agreement between the calculated and experimental results.

Acknowledgements

The financial support of the Technology Development Centre (TEKES) during project "Development of simulation models for continuous casting" is gratefully acknowledged.

Appendix A. Substitutional solution model and data

The molar Gibbs energy of a binary substitutional solution phase is expressed as

$$G^{\phi} = \sum_{i=1}^{2} x_i^{\phi}\left[({}^{0}G_i^{\phi} - {}^{0}G_i^{\theta}) + ({}^{0}G_i^{\theta} - H_i^{\mathrm{SER}})\right] + RT\sum_{i=1}^{2} x_i^{\phi}\ln x_i^{\phi} + {}^{\mathrm{E}}G^{\phi}, \quad (A.1)$$

where $i = 1$ denotes Cu and $i = 2$ denotes component B. The first and the second summations represent the mechanical mixture of pure components and the contribution of mixing entropy, respectively. The third term, ${}^{\mathrm{E}}G^{\phi}$, is the Gibbs excess energy expressed for a binary Cu–B phase as

$${}^{\mathrm{E}}G^{\phi} = (1 - x_{\mathrm{B}}^{\phi})x_{\mathrm{B}}^{\phi}L_{\mathrm{CuB}}^{\phi}. \quad (A.2)$$

In Eq. (A.1), ${}^{0}G_i^{\phi} - {}^{0}G_i^{\theta}$ is the Gibbs energy of a pure component in phase ϕ expressed relative to the reference phase of the component, θ, and ${}^{0}G_i^{\theta} - H_i^{\mathrm{SER}}$ is the Gibbs energy of the component in its reference phase expressed relative to the enthalpy of the SER state [92] (the reference phase for the component at 298.15 K). In Eq. (A.2), parameter L_{CuB}^{ϕ} describing the interaction between Cu and component B can be a function of temperature and composition. Finally, knowing the molar Gibbs energy of Eq. (A.1), the chemical potential of component i can be solved as

$$\mu_i^{\phi} = G^{\phi} + \partial G^{\phi}/\partial x_i^{\phi} - \sum_{j=1}^{2} x_j^{\phi}(\partial G^{\phi}/\partial x_j^{\phi}), \quad (A.3)$$

where $i = 1$ denotes Cu and $i = 2$ denotes component B. In the CASBOA model, the chemical potentials are used to determine the thermodynamic equilibrium at the fcc/L interface, as shown by

Eqs. (1) and (2). In addition, parameter G^{ϕ} of Eq. (A.1) is used to calculate enthalpy and heat capacity as shown by Eqs. (5) and (6), and parameter ${}^{E}G^{\phi}$ of Eq. (A.2) for liquid is used to calculate the liquid viscosity as shown by Eqs. (15) and (16). Note that in any derived equation, one can set $x_{Cu} = 1 - x_B$.

The present databank of the CASBOA model contains thermodynamic substitutional solution data for the liquid and fcc phases of binary Cu–B systems with B = Ag, Al, Ni, P, Sn and Zn. The reference phases (θ) of the components are the same as those of the SGTE database [92]. The adopted

Table 13
Gibbs energies (J/mol) of pure components in their reference phases (θ) expressed relative to the SER state (H^{SER}) [91][a]

i	Set	Function	Temperature range (K)
Cu	1	$-13542.03 + 183.8038T - 31.38T\ln T + 3.642E + 29/T^9$	$T < 3200$
	2	$-7770.458 + 130.4852T - 24.11239T\ln T - 2.65684E-03T^2$ $+1.29223E-07T^3 + 52478/T$	$T < 1358$
Ag	1	$-15095.25 + 190.2664T - 33.472T\ln T + 1.412E + 29/T^9$	$T < 3000$
	2	$-7209.512 + 118.202T - 23.84633T\ln T - 1.790585E-03T^2$ $-3.98587E-07T^3 - 12011/T$	$T < 1235$
Al	1	$-11278.38 + 188.6841T - 31.74819T\ln T - 1.231E + 28/T^9$	$T < 2900$
	2	$-6651.502 + 107.1T - 19.35411T\ln T - 1.033351E-02T^2$ $+1.833441E-06T^3 - 1.823694E-19T^7 + 8839.191/T$ (S)	$T < 933$
Ni	1	$-27840.65 + 279.135T - 43.1T\ln T + 1.12754E + 31/T^9$	$T < 3000$
	2	$-5179.159 + 117.854T - 22.096T\ln T - 0.0048407T^2$	$T < 1728$
P	1	$-8093 + 135.89T - 26.326T\ln T$	$T < 3000$
	2	$-9587.448 + 152.3415T - 28.73353T\ln T + 1.715669E-03T^2$ $-2.2829E-07T^3 + 172966/T$	$T < 1000$
Sn	1	$-4215.867 + 97.32976T - 22.42609T\ln T - 3.991321E-03T^2$ $+5.022911E-07T^3 - 7.856303E-22T^7 - 504285/T$ (S)	$T < 2000$
	2	$-5855.135 + 65.44331T - 15.961T\ln T - 0.0188702T^2$ $+3.121167E-06T^3 - 61960/T$	$T < 505$
Zn	1	$-11070.56 + 172.3457T - 31.38T\ln T + 4.7051E + 26/T^9$	$T < 3000$
	2	$-7285.787 + 118.4701T - 23.70131T\ln T$ $-1.712034E-03T^2 - 1.264963E-06T^3$	$T < 693$

[a] The parameter equals to expression ${}^{0}G_i^{\theta} - H_i^{SER}$ of Eq. (A.1). For each component, two functions (sets 1 and 2) are given. Symbol S denotes a simplified expression.

Table 14
Gibbs energies (J/mol) of pure components in the liquid phase expressed relative to their reference phases (θ) [91][a]

i	Set	Function	Temperature range (K)
Cu	1	$13495.48 - 9.922344T - 3.642E + 29/T^9$	$T < 3200$
	2	$12964.74 - 9.511904T - 5.849E - 21T^7$	$T < 1358$
Ag	1	$11508.14 - 9.301747T - 1.412E + 29/T^9$	$T < 2900$
	2	$11025.08 - 8.891021T - 1.034E - 20T^7$	$T < 1235$
Al	1	$10482.38 - 11.25397T + 1.231E + 28/T^9$	$T < 2900$
	2	$11005.03 - 11.84187T + 7.934E - 20T^7$	$T < 933$
Ni	1	$18290.88 - 10.537T - 1.12754E + 31/T^9$	$T < 3000$
	2	$16414.69 - 9.397T - 3.82318E - 21T^7$	$T < 1728$
P	1	$860.626 - 2.584958T$	$T < 3000$
	2	$2354.999 - 19.04961T + 2.40753T\ln T$ $-1.715669E-03T^2 + 2.2829E-07T^3 - 172966/T$	$T < 1000$
Sn	1	$6971.587 - 13.81438T + 1.2307E + 25/T^9$	$T < 3000$
	2	$7103.092 - 14.08777T + 1.47031E - 18T^7$	$T < 505$
Zn	1	$7450.123 - 10.73623T - 4.70657E + 26/T^9$	$T < 3000$
	2	$7157.27 - 10.29234T - 3.58652E - 19T^7$	$T < 693$

[a] The parameter equals to expression ${}^{0}G_i^{L} - {}^{0}G_i^{\theta}$ of Eq. (A.1). For each component, two functions (sets 1 and 2) are given.

Table 15
Gibbs energies (J/mol) of pure components in the fcc phase expressed relative to their reference phases (θ) [92][a]

i	Set	Function	Temperature range (K)
Cu	1	0	$T < 3200$
Ag	1	0	$T < 3000$
Al	1	0	$T < 2900$
Ni	1	0	$T < 3000$
P	1	$-74027.9 + 936.5915T - 133.1811T\ln T + 8.020637E-02T^2$ $-9.02059E-06T^3 + 8.898341E-21T^7 + 1.13517E+07/T$ (*S*)	$T < 2000$
	2	$23542.78 - 63.58124T + 10.37041T\ln T - 5.109667E-03T^2$ $-1.184678E-06T^3 + 7.780598E-20T^7 - 254210.7/T$ (*S*)	$T < 1000$
Sn	1	$4150 - 5.2T$	$T < 3000$
Zn	1	$2969.82 - 1.56968T$	$T < 3000$

[a] The parameter equals to expression ${}^0G_i^{\mathrm{fcc}} - {}^0G_i^{\mathrm{B}}$ of Eq. (A.1). For each component, one or two expressions are given. Symbol *S* denotes a simplified expression.

Table 16
Binary interaction parameters $L_{\mathrm{CuB}} = f(T, x_{\mathrm{B}})$ (J/mol) in the liquid phase

CuB	Expression	References
Cu–Ag	$(15200 - 2.4T) + (1800 - .8T)(1 - 2x_{\mathrm{Ag}}) + (-1.5T)(1 - 2x_{\mathrm{Ag}})^2$	[94]
Cu–Al	$(-66622 + 8.1T) + (-46800 + 90.8T - 10T\ln T)(1 - 2x_{\mathrm{Al}}) + (-2812)(1 - 2x_{\mathrm{Al}})^2$	[95]
Cu–Ni	$(12049 + 1.299T) + (-1862 + .942T)(1 - 2x_{\mathrm{Ni}})$	[95]
Cu–P	$(-314121 + 162.321T) + (120596 - 98.609T)(1 - 2x_{\mathrm{P}})^2$	[96]
Cu–Sn	$(-9003 - 5.838T) + (-20100 + 3.637T)(1 - 2x_{\mathrm{Sn}}) + (-10528)(1 - 2x_{\mathrm{Sn}})^2$	[93]
Cu–Zn	$(-40696 + 12.653T) + (4403 - 6.554T)(1 - 2x_{\mathrm{Zn}}) + (7818 - 3.254T)(1 - 2x_{\mathrm{Zn}})^2$	[95]

Table 17
Binary interaction parameters $L_{\mathrm{CuB}} = f(T, x_{\mathrm{B}})$ (J/mol) in the fcc phase

CuB	Expression	References
Cu–Ag	$(40600 - 15T) + (-9000 + 12T)(1 - 2x_{\mathrm{Ag}})$	[94]
Cu–Al	$(-53520 + 2T) + (-38590 + 2T)(1 - 2x_{\mathrm{Al}}) + (1170)(1 - 2x_{\mathrm{Al}})^2$	[95]
Cu–Ni	$(8048 + 3.422T) + (-2041 + .997T)(1 - 2x_{\mathrm{Ni}})$	[95]
Cu–P	$(-168456 + 45.002T)$	[96]
Cu–Sn	$(-10672 - 1.484T) + (-15331 + 6.954T)(1 - 2x_{\mathrm{Sn}})$	[93]
Cu–Zn	$(-42804 + 10.023T) + (2936 - 3.053T)(1 - 2x_{\mathrm{Zn}}) + (9034 - 5.393T)(1 - 2x_{\mathrm{Zn}})^2$	[95]

data are based on the recent thermodynamic assessments of copper-based systems [92–96] and are shown in Tables 13–17. In Tables 13 and 15, the parameter expression is equipped with symbol *S* to indicate that the temperature function of the original parameter expression [92] has been simplified.

Appendix B. Optimised solute diffusion data and its validation

The diffusion coefficient of the solute, $D_{\mathrm{B}}^{\phi}(\mathrm{cm}^2/\mathrm{s})$, is typically presented by the Arrhenius equation as

$$D_{\mathrm{B}}^{\phi} = D_{\mathrm{B}}^{0\phi} \exp(-Q_{\mathrm{B}}^{\phi}/RT), \tag{B.1}$$

where $D_{\mathrm{B}}^{0\phi}$ is the pre-exponential diffusion coefficient (cm^2 /s), Q_{B}^{ϕ} is the activation energy (J/mol), R is the gas constant (8.3145 J/Kmol) and T is temperature (K). As this equation takes no account of the alloy composition, a specific composition term was recently added in it [6], based on the experimental data [97–102]. For binary copper alloys containing Ag, Al, Ni, P, Sn or Zn, the new equation takes the form

$$D_{\mathrm{B}}^{\phi} = D_{\mathrm{B}}^{0\phi} \exp\left(-\frac{Q_{\mathrm{B}}^{\phi} + b_{\mathrm{B}}x_{\mathrm{B}}}{RT}\right), \tag{B.2}$$

Table 18
Parameters D_B^0, Q_B and b_B of Eq. (B.2) for the calculation of diffusion coefficients D_B in binary fcc copper alloys

Solute B	D_B^0 (cm^2/s)	Q_B (J/mol)	b_B (J/mol)
Ag	0.1928	183 509	−110 127
Al	0.5223	196 153	−173 705
Ni	0.3603	214 170	50 293
P	0.00305	136 000	0
Sn	0.0393	160 548	−241 988
Zn	0.2573	188 118	−107 328

Table 19
Average error between the experimental and calculated solute diffusion data in binary fcc copper alloys (shown also are the number of the experimental data points, and the composition and temperature ranges of the data)

Cu–B	Data points	at.% B	T (°C)	Error (%)
Cu–Ag	45	0–2	701–1000	0.3
Cu–Al	42	0–10	704–1004	0.2
Cu–Ni	27	0–40	947–1054	0.3
Cu–Sn	41	0–7	731–832	0.3
Cu–Zn	25	6–27	700–910	0.6

where x_B is the solute composition in mole fraction and b_B is a coefficient describing the effect of solute on its activation energy (J/mol). The optimised parameters of Eq. (B.2) for binary fcc copper alloys are presented in Table 18. Table 19 shows the average error (in %) between the experimental and calculated solute diffusion data in the fcc phase. The average error term in the last column is defined as $100 \cdot \Sigma(|\log(D_i^{exp}) - \log(D_i^{cal})|/|\log(D_i^{exp})|)/n$, where the summation covers the n experimental data points available for the system. The agreement is relatively good the average error being less than 0.5 pct for any system. A complete description of this optimisation is shown in the earlier report [6].

Appendix C. Optimised dendrite arm spacing data and its validation

The secondary dendrite arm spacing d_2(μm) depends on the cooling rate $\dot{T}$(°C/s) according to the following empirical equation [103]:

$$d_2 = a \cdot \dot{T}^{-n}, \tag{C.1}$$

where a and n are the constants. The experimental value of exponent n typically varies between 0.33 and 0.5 whereas the theoretical value is 1/3 [104]. As this equation takes no account of the alloy composition, a specific composition term was recently added in it [6], based on experimental data [91,105,106,90,107–109]. For binary copper alloys containing Ag, Al, Ni, P, Sn or Zn, the new equation takes the form

$$d_2 = 175\ \dot{T}^{-0.33} \exp(a_B C_B^{b_B}), \tag{C.2}$$

where C_B is the solute composition in wt%, and a_B and b_B are the optimised parameters presented in Table 20. Table 21 shows the average error (in %) between the experimental and calculated dendrite arm spacing data in binary copper alloys. The average error term in the last column is defined as $100 \cdot \Sigma(|d_2^{exp} - d_2^{cal}|/d_2^{exp})/n$, where the summation covers the n experimental data points available for the alloy. The agreement is reasonable although more data would have been necessary to get a

Table 20
Parameters a_B and b_B of Eq. (C.2) for the calculation of the secondary dendrite arm spacing in binary copper alloys

Solute B	a_B	b_B
Ag	−0.9725	0.3
Al	−0.1718	0.4
Ni	−0.3952	0.4
P	−0.3	1
Sn	−0.1	1
Zn	−0.3096	0.4

Table 21
Average error between the experimental and calculated dendrite arm spacing data in binary copper alloys (shown also are the number of the experimental data points, and the composition and cooling rate ranges of the data)

Cu–B	Data points	wt% B	$\dot{T}$ (°C/s)	Error (%)
Cu–Ag	3	0.5	0.25–2	2.1
Cu–Ag	3	1	0.25–2	2.1
Cu–Ag	3	5	0.25–2	8.2
Cu–Ni	1	0.9	0.83	33.7
Cu–Ni	3	30	0.2–2	5.0
Cu–P	3	0.022	0.1–1.2	4.1
Cu–Sn	2	10	0.37–0.85	2.1
Cu–Sn	1	19.3	590	6.4
Cu–Zn	1	1	0.83	27.5
Cu–Zn	6	35	56–233	17.6
Cu–Zn	3	36.2	0.1–0.8	13.8

reliable description at a larger cooling rate region. A complete description of this optimisation is shown in the earlier report [6].

References

[1] M. Rappaz, Int. Mat. Rev. 34 (1989) 93.
[2] M.C. Flemings, in: Proceedings of the Elliott Symposium on Chemical Process Metallurgy, Cambridge, MA, June 10–13, 1984, The Iron and Steel Society, Warrendale, PA, 1991, p. 253.
[3] J. Miettinen, Metall. Trans. A 23A (1992) 1155.
[4] J. Miettinen, Metall. Trans. B 28B (1997) 281.
[5] J. Miettinen, Thermodynamic–kinetic simulation of solidification and phase transformations in steels, Report TKK-MK-78 Helsinki University of Technology Publications in Materials Science and Metallurgy, Espoo, 1999.
[6] J. Miettinen, Diffusion and microstructure data for copper alloys, Report TKK-MK-101 Helsinki University of Technology Publications in Materials Science and Metallurgy, Espoo, 2000.
[7] M. Hillert, in: D.V. Doane, J.S. Kirkaldy (Eds.), Hardenability Concepts with Application to Steel, TMS-AIME, Warrendale, PA, 1978, p. 5.
[8] J. Miettinen, Enthalpy data for binary copper alloys, Report TKK-MK-100 Helsinki University of Technology Publications in Materials Science and Metallurgy, Espoo, 2000.
[9] I. Barin, Thermochemical data of pure substances, Part I VCH Verlagsgesellschaft mbH, D-6940 Weinheim, Germany, 1989.
[10] K. Parameswaran, G. Healy, Metall. Trans. B 9B (1978) 657.
[11] W.R. Bitler, K.P. Moll, Thermodynamic properties of copper-base alloys, INCRA project No. 245 Department of Materials Science and Engineering, The Pennsylvania State University, University Park, Pennsylvania, 1981.
[12] M. Kawakami, Sci. Rept. Tohoku Imp. Univ. 19 (1930) 521.
[13] H.-O. von Samson-Himmelstjerna, Z. Metallkde 28 (1936) 197.
[14] W. Oelsen, W. Middel, Mitt. KWI für Eisenforsch 19 (1937) 1.
[15] R.A. Oriani, W.K. Murphy, J. Phys. Chem. 62 (1958) 199.
[16] M.G. Benz, J.F. Elliott, Trans. AIME 230 (1964) 706.
[17] R.N. Dokken, J.F. Elliott, Trans. Met. Soc. AIME 233 (1965) 1351.
[18] B. Predel, R. Mohs, Arch. Eisenhüttenw. 42 (1971) 575.
[19] Y. Tozaki, Y. Iguchi, S. Ban-Ya, T. Fuwa, in: Chemical Metallurgy of Iron and Steel, Proceedings of the International Symposium on Met. Chem. Applications in Ferrous Met., University of Sheffield, 1971. Iron and Steel Institute, London, 1973, p. 130.
[20] S. Takeuchi, O. Uemura, S. Ikeda, Sci. Rep. Tohoku Imp. Univ. 25A (1974) 41.
[21] K. Itagaki, A. Yazawa, Trans. Japan Inst. Met. 16 (1975) 679.
[22] M.J. Pool, B. Predel, E. Schultheiss, Thermochim. Acta 28 (1979) 349.
[23] O.J. Kleppa, S. Watanabe, Metall. Trans. B 13B (1982) 391.
[24] J. Tomiska, A. Neckel, Int. J. Mass Spectrom. Ion Phys. 47 (1983) 223.
[25] J.J. Lee, B.J. Kim, W.S. Min, J. Alloys Compounds 202 (1993) 237.
[26] U.K. Stolz, I. Arpshofen, F. Sommer, Z. Metallkde. 84 (1993) 552.
[27] K. Fitzner, Q. Guo, J. Wang, O. Kleppa, J. Alloys Compounds 291 (1999) 190.
[28] F. Körber, W. Oelsen, Mitt. KWI für Eisenforsch. 19 (1937) 209.
[29] Z. Weibke, Z. Anorg. Chem. 323 (1937) 289.
[30] R.A. Oriani, W.K. Murphy, Acta Metall. 8 (1960) 23.
[31] O.J. Kleppa, R.C. King, Acta Metall. 10 (1962) 1183.
[32] R.L. Orr, B.B. Argent, Trans. Faraday Soc. 61 (1965) 2126.
[33] L. Elford, F. Müller, O. Kubaschewski, Ber. der Bunsengesellschaft 73 (1969) 601.
[34] I. Katayama, H. Shimatani, Z. Kozuka, Nippon Kinzoku Gakk. 37 (1973) 509.
[35] F. Forsler, G. Tschentke, Z. Metallkde. 32 (1940) 191.
[36] H. Masumuto, H. Saito, M. Takahashi, Nippon-Kinzoku-Gakkai Shi 18 (1954) 98.
[37] R.D. Pehlke, A. Jeyarajan, H. Wada, Summary of thermal properties for casting alloys and mold materials, Report NSF/MEA-82028 Department of Materials and Metallurgical Engineering, University of Michigan, 1982.
[38] F. Wust, A. Meuthin, R. Durrer, Forsch. Gebiete Ingenieurw, WDI – Forschungsch, 1918, p. 204.
[39] J.F. Elliott, M. Gleiser, Thermochemistry for Steelmaking, vol. 1, Addison-Wesley, Reading, MA, 1960.
[40] R. Hultgren, R.L. Orr, D. Andersson, K.K. Kelley, Selected Values of Thermodynamic Properties of Metals and Alloys, Wiley, New York, 1963.
[41] R.P. Tye, R.W. Hayden, High Temp. High Press. 11 (1979) 597.
[42] E.A. Brandes, G.B. Brook, Smithells Metals Reference Book, seventh ed., Butterworth-Heinemann, Oxford, 1992.
[43] R.C. Weast, Handbook of Chemistry and Physics, 53rd ed. The Chemical Rubber, Cleveland OH, 1973.
[44] K. Dies, Kupfer und Kupferlegierungen in der Technik, Springer, Berlin, 1967.
[45] C.Y. Ho, M.W. Ackerman, K.Y. Wu, S.G. Oh, T.N. Havill, J. Phys. Chem. Ref. Data 7 (1978) 959.
[46] Metals Handbook, tenth ed., vol. 2, American Society for Metals, Metals Park, OH, 1990.
[47] K. Bornemann, F. Sauerwald, Z. Metallkd. 14 (1922) 145.
[48] L.D. Lucas, Compt. Rend. 252 (1961) 2526.
[49] M.G. Frohberg, R. Weber, Arch. Eisenhüttenwes 35 (1964) 877.
[50] S. Watanabe, T. Saito, Trans. JIM 13 (1972) 186.

[51] R.F.A. Freeman, The surface tension of copper and its alloys, Report R347/10/September 1973. Physics Department, Fulmer Research Institute, Stoke Poges, England, 1973.
[52] R.F.A. Freeman, The surface tension of copper and its alloys, Report R347/2/October 1971 Physics Department, Fulmer Research Institute, Stoke Poges, England, 1971.
[53] R.F.A. Freeman, The surface tension of copper and its alloys, Report R347/6/September 1972 Physics Department, Fulmer Research Institute, Stoke Poges, England, 1972.
[54] R.F.A. Freeman, The surface tension of copper and its alloys, Report R347/11/January 1975 Physics Department, Fulmer Research Institute, Stoke Poges, England, 1975.
[55] C.O. Ruud, M.T. Hepworth, J.M. Fernandez, Metall. Trans. B 6B (1975) 351.
[56] W.B. Pearson, A Handbook of Lattice Spacings and Structures of Metals and Alloys, Pergamon Press, London, 1958.
[57] E. Schmid, G. Siebel, Z. Phys. 85 (1932) 36.
[58] A.J. Bradley, P. Jones, J. Inst. Metals 51 (1933) 131.
[59] I. Obinata, G. Wassermann, Naturwissenschaften 21 (1933) 382.
[60] E.A. Owen, L. Pickup, Z. Krist. 88 (1934) 116.
[61] E.A. Owen, J. Rogers, J. Inst. Metals 57 (1935) 257.
[62] E.A. Owen, J. Iball, J. Inst. Metals 57 (1935) 267.
[63] C. Haase, F. Pawlek, Z. Metallkd. 28 (1936) 73.
[64] W. Hume-Rothery, G.F. Lewin, P.W. Reynolds, Proc. Roy. Soc. A 157 (1936) 167.
[65] S.T. Konobeevskii, W.P. Tarassova, Acta Physiochim. URSS 6 (1937) 781.
[66] J.C. Mertz, C.H. Mathewson, Trans. AIME 124 (1937) 59.
[67] E.A. Owen, E.W. Roberts, Phil. Mag. 27 (1939) 294.
[68] K.W. Andrews, W. Hume-Rothery, Proc. Roy. Soc. A 178 (1941) 464.
[69] W. Hume-Rothery, K.W. Andrews, J. Inst. Metals 68 (1942) 19.
[70] A.P. Guljaev, E.F. Trusova, Z. Tekh. Fiz. 20 (1950) 66.
[71] B.R. Coles, J. Inst. Metals 84 (1955) 346.
[72] P.H. Stirling, G.V. Raynor, J. Inst. Metals 84 (1955) 57.
[73] A.F. Anderson, Trans Amer. Soc. Met. 212 (1958) 259.
[74] M.S. Wechsler, R.H. Kemohan, J. Phys. Chem. Solids 7 (1958) 307.
[75] G.B. Mitra, S.K. Mitra, Indian J. Phys. 37 (1963) 462.
[76] M.K. Asundi, D.R.F. West, J. Inst. Metals 94 (1966) 327.
[77] M. Kantola, E. Tokola, Ann. Acad. Sci. Fenn. 223A (1967) 1.
[78] F. Lihl, H. Ebel, A. Reichl, A. Kaminitschek, Z. Metallkd. 59 (1968) 735.
[79] S.S. Rao, T.R. Anantharaman, Z. Metallkd. 60 (1969) 312.
[80] A.K. Jena, D. Gulati, T.R. Ramachandran, Z. Metallkd. 72 (1981) 847.
[81] D. Sichen, J. Bygden, S. Seetharaman, Metall. Mater. Trans. B 25B (1994) 519.
[82] E. Rothwell, J. Inst. Metals 90 (1961) 389.
[83] T. Iida, Z. Morita, S. Takeuchi, J. Jpn. Inst. Metals 39 (1975) 1169.
[84] C.O. Ruud, D. Chandra, J.M. Fernandez, M.T. Hepworth, Metall. Trans. B 7B (1976) 497.
[85] T. Iida, A. Satoh, S. Ishiura, S. Ishiguro, Z. Morita, J. Jpn. Inst. Metals 44 (1980) 443.
[86] Y. Kawai, Y. Shiraishi, Handbook of Physico-Chemical Properties at High Temperatures, The Iron and Steel Institute of Japan, 1988, p. 93.
[87] B. Sikora, M. Zielinski, K. Orecki, Rudy Metale Niezelazne 17 (1972) 20.
[88] Y. Kawai, M. Anabuki, J. Jpn. Inst. Metals 37 (1973) 664.
[89] V.I. Volkov, Y.U.V. Fisher, N.N. Novikova, S.E. Vaisburd, Izv. Vuz. Tsvetnaya Met. 5 (1984) 63.
[90] L. Bäckerud, L-M. Liljenvall, H. Steen, Solidification characteristics of some copper alloys. International Copper Research Association, Stockholm, 1982.
[91] A.T. Dinsdale, CALPHAD 15 (1991) 317.
[92] J.-H. Shim, C.-S. Oh, B.-J. Lee, D.N. Lee, Z. Metallkd. 87 (1996) 205.
[93] S-S. Lim, J.E. Tibbals, P. Rossiter, Z. Metallkd. 88 (1997) 236.
[94] I. Ansara, A.T. Dinsdale, M.H. Rand, COST 507 – Thermochemical Database for Light Metal Alloys, vol. 2, European Communities, Belgium, 1998.
[95] J. Miettinen, Thermodynamic description of Cu–P system, Internal report, Laboratory of Metallurgy, Helsinki University of Technology, Espoo, 2000.
[96] R. Reisnick, R. Baluffi, J. Metals 7 (1955) 1004.
[97] A. Vignes, C.E. Birchenall, Acta Metall. 16 (1968) 1117.
[98] H. Oikawa, H. Takei, S. Karashima, Metall. Trans. 4 (1973) 653.
[99] N. Matsuno, H. Oikawa, Metall. Trans. A 6A (1975) 2191.
[100] H. Oikawa, A. Hosoi, Scripta Met. 9 (1975) 823.
[101] P. Spindler, K. Nachtrieb, Phys. Stat. Sol. (a) 37 (1976) 449.
[102] T.F. Bower, H.D. Brody, H.D. Flemings, Trans. AIME 624 (1966) 624.
[103] W. Kurz, D.J. Fisher, Fundamentals of Solidification, third ed., Trans. Tech. Publications, Aedermannsdorf, Switzerland, 1989, p. 85.
[104] A. Gibula, Review of metallurgical factors influencing the quality of copper and copper alloy castings, in: BNFMRA International Conference on the Control of the Composition and Quality of Copper and Copper Alloy Castings for Fabrication Düsseldorf, October, 1967.
[105] L. Bäckerud, L.-M. Liljenvall, J. Inst. Metals 100 (1972) 357.
[106] L. Bäckerud, L.-M. Liljenvall, The solidification characteristics of 12 commercial copper-base alloys, INCRA Report 165A Swedish Institute for Metals Research, Stockholm, 1973.
[107] K. Kusabiraki, K. Imai, J. Jpn. Inst. Met. 47 (1983) 896.
[108] J. Liu, N. Jacobson, H. Fredriksson, Report TRITA-MAC-0395 Materials Research Center, Royal Institute of Technology, Stockholm, 1989.
[109] K. Härkki, J. Miettinen, Metall. Mater. Trans. B 30B (1999) 75.